Kinetics of electron-hole droplet clouds: The role of thermalization phonons

R. S. Markiewicz
General Electric Corporate Research and Development, Schenectady, New York 12301
(Received 3 May 1979)

This paper presents a detailed analysis of the phonon wind which is responsible for the large cloud of electron-hole droplets often observed in Ge. The phonons are separated into two categories: T phonons, produced by the initial thermalization of the hot carriers, and R phonons, produced when an electron-hole pair recombine nonradiatively. It is shown that, while most of the T-phonon energy is effectively lost in an initial optical-phonon cascade, there is a residual energy given off to acoustic phonons when the carriers have cooled to within a single optical-phonon energy of the band edge. These phonons, which represent less than one percent of the total phonon energy, produce all of the characteristic features of the phonon wind. Without the T phonons, the cloud density would not saturate, but would continue to grow as the laser power increased, and the cloud volume would not increase with power. Also, since the T phonons reach steady state in essentially the thermalization time, the phonon wind is present in full force almost from the moment the drops condense, causing a rapid initial growth of the cloud. In addition to kinetic equations describing cloud buildup, more detailed models of the thermalization process are presented, in order to estimate the time evolution of the condensation and the magnitude of the wind. The theoretical prediction is in good agreement with experiments (except at high-absorption-power pulsed experiments, in which the wind is greatly enhanced). The number of R phonons is harder to estimate; because they are spread out over the entire volume of the cloud, their effects are greatly diluted, and they make very little contribution to the characteristic features of the phonon wind. An analysis of previous experiments suggests that R phonons may be as much as five times as numerous as T phonons.

I. INTRODUCTION

Keldysh[1] showed that electron-hole droplets (EHD's)[2] can easily be moved through large distances by a stream of nonequilibrium phonons. Furthermore, he suggested that such nonequilibrium phonons could be responsible for the characteristic spatial distribution[3,4] of EHD's in photoexcited Ge which cannot be explained by simple diffusion of the droplets. The EHD distribution does not decay exponentially away from the illuminated crystal surface with a characteristic diffusion length. Instead, the droplet density remains approximately constant throughout a *cloud* whose volume increases approximately linearly with light excitation level. This cloud, Keldysh showed, is produced by a wind of phonons which are created concomitantly with the electron-hole (e-h) pairs and travel ballistically through the crystal.

Several experiments[4-6] have confirmed that EHD's can easily be moved by streams of phonons, but there are questions remaining as to the origin of the phonons responsible for creating the usual EHD cloud. In particular, it is not clear whether these phonons are produced during the initial thermalization of hot carriers near the crystal surface where the light is absorbed, or if they are produced in the EHD's themselves, during nonradiative recombination. This paper will show that these two types of phonons, thermalization and recombination (abbreviated T and R) lead to dramatically different predictions for the dynamic behavior of the EHD cloud, and that the characteristic features of the cloud are due to thermalization phonons.

A. Classification of phonons

The nonequilibrium phonons are produced as hot electrons and holes cool down toward the lattice temperature. There are two independent sources of hot carriers: (1) the e-h pair is initially created by absorbing a photon of energy $h\nu$. The excess energy $h\nu - E_g$ (E_g is the gap energy) is emitted as phonons. (2) An e-h pair may recombine nonradiatively, giving up the excess energy E_g to a single carrier (Auger process). This carrier must then thermalize by processes similar to case (1). The phonons produced in these two processes, called T (thermalization) or R (recombination) phonons, respectively, differ in two important features. First, the T phonons are spatially localized near the surface where the light is initially absorbed, while R phonons are produced uniformly throughout the cloud. Secondly, the T phonons reach steady state in a thermalization time, ~10 nsec, while the number of EHD's, and consequently of R phonons, reaches steady state only after the much slower time $\tau_0 = 40$ μsec. Each of these differences leads to very different predictions of cloud properties, and the experimental evidence strongly confirms the importance of T phonons.

Both of the above mechanisms rely on hot carriers to heat the EHD's to temperatures slightly above the lattice temperatures, from which they cool down by emitting low-energy acoustic phonons. In a recent experiment[6] the drops were heated directly (by absorbing far-infrared light), and the phonons detected by an enhancement of the EHD velocity. The enhancement is of the correct order of magnitude, confirming the importance of the present mechanisms.

B. Kinetic equations

Keldysh approached the problem of the phonon wind by postulating a form for the force between two EHD's due to the emission and absorption of nonequilibrium phonons, then setting up and solving the kinetic equations of the droplets moving under such a force. He showed that, if the phonons moved ballistically, the magnitude of the force would decrease as $1/r^2$, due solely to geometric spreading. He then formulated the theory on an electrical analogy, representing the phonon-wind force as an effective charge ρ on a drop.

Keldysh did not consider the origin of these nonequilibrium phonons in any detail. In deriving an order-of-magnitude estimate of ρ, he assumed that they are R phonons, hence equally present in all drops. Yet in analyzing the kinetic equations he made the simplifying assumption that all the phonons emanate from a point source—at the sample surface, where the laser is focused. The error involved in this assumption for R phonons is immediately obvious by a comparison with gravitational theory. The force of gravity at any point *outside* the earth can be calculated by assuming the mass of the earth is concentrated at the center. Using this formula at a point r *inside* the earth overestimates the gravitational force by a factor $(r_e/r)^3$, where r_e is the radius of the earth. Similarly, in the present problem, the R phonon wind is reduced in magnitude by the analogous factor $(r_c/r)^3$, with r_c the radius of the cloud. On the other hand, T phonons do not have such a reduction factor; they are produced within a very small radius (~100 μm) of the laser spot, and, as far as the cloud is concerned, constitute a true point source. Because of the volume-reduction factor, the T phonons play the dominant role in cloud formation even if there are numerically many more R phonons.

In Sec. II the kinetic equations of Keldysh are generalized by separately including R and T phonons. Instead of a charge density ρ, the force of the wind is written in terms of two parameters γ_R and γ_T. These differ from ρ only in the normalization; for $\gamma_R = 0$, $\rho^2 = n_0^2 m \gamma_T / \tau_{ep} \tau_0$, where n_0 is the pair density inside an EHD, m is the mass of an e-h pair, τ_0 is the pair-recombination time, and τ_{ep} is the electron-phonon collision rate. The results of Sec. II confirm the above discussion. If there are no T phonons, the characteristic cloud does not form no matter how large γ_R is; most of the EHD remain localized near the laser spot. On the other hand, only a few T phonons are needed to produce the characteristic cloud shape.

T phonons are also important in understanding the kinetics of buildup of the cloud. These phonons reach steady state in approximately the thermalization time of the carriers, much faster than the EHD recombination time. Hence the wind appears strongest just after the EHD form, when they are localized near the crystal surface. This accounts for the rapid initial spreading of the cloud observed experimentally.[7] Section III gives time-dependent solutions to the cloud kinetic equations, in reasonable agreement with experiment. The pulsed experiments of Damen and Worlock[8] and Durandin *et al.*[9] can also be understood, although at these intense pumping levels the wind appears noticeably stronger.

C. Origins of the phonon wind

Section IV attempts to go beyond the kinetic equations and to estimate the magnitudes of γ_T and γ_R—that is, to understand the origins of the phonons which produce the wind. This involves a detailed consideration of electron-phonon, electron-electron, and phonon-phonon interactions. Numerous approximations preclude complete solution, but the problem is reduced to the calculation of a few basic parameters, and good agreement with experiment is obtained with a reasonable choice of values for these parameters.

The problem of calculation of the γ's can be subdivided into three parts: (1) estimating the initial heat input into the EHD system, (2) calculating the phonon emission spectrum, and (3) calculating the probability of absorption once the phonon spectrum is known. Step (3) is carried out in a previous paper,[10] and step (2) is no more difficult (Appendix B). The problem lies entirely in step (1).

The essence of the difficulty is that the EHD's *are transparent to most of the phonon wind.* This is because EHD's interact strongly only with acoustic phonons of wave number $q < 2k_F$, where $k_F \sim 10^6$ cm^{-1} is the Fermi wave vector of the carriers. Most of the energy of the hot carriers is very rapidly emitted in an optical phonon cascade. *Only when the excess carrier energy is smaller than the energy of a single optical phonon does*

acoustic phonon emission become an important thermalization process. It is mainly those phonons in this tail of the thermalization which contribute to the phonon wind[11] (Sec. IV A). The optical-phonon cascade involves between 10 and 50 phonons, depending on the initial carrier energy; the parameter of importance to the phonon wind is ΔE_0, the average energy of an e-h pair at the end of this optical-phonon cascade. This number cannot be easily estimated, beyond the fact that it is less than an optical-phonon energy (~35 meV), but a value of ~10 meV gives good agreement with experiment. In fact, γ_T is approximately linear in ΔE_0, giving an experimental value $\Delta E_0 \sim 5-15$ meV.

It may be thought at this point that T and R processes should follow virtually the same sequence and that γ_R and γ_T should be nearly the same size (or at least, both proportional to some $\Delta E_0 < 35$ meV). There is one factor which complicates the R-phonon sequence, allowing the possibility that $\gamma_R \gg \gamma_T$. Inside an EHD the pair density $n_0 = 2 \times 10^{17}$ cm^{-3} is sufficiently high that a hot carrier can lose energy via electron-electron collisions (either single carrier or plasmon emission) instead of by optical-phonon emission.[12] A rough estimate[13] shows that the former may be important inside EHD. Any energy transferred to the carrier system as a whole will ultimately be dissipated as low-energy acoustic phonons, thereby enhancing γ_R. Since the average density in a cloud is ~10^{15} cm^{-3}, carrier-carrier collisions will be much less significant for T phonons. The enhancement of γ_R cannot be easily estimated, particularly since Auger carriers have a large probability of escaping from an EHD (Ref. 2, p. 171).

There is, finally, one more possible contribution to the phonon wind. Whereas the optical (and high-energy acoustic[14]) phonons do not interact directly with EHD's, they do decay (via three-phonon processes) to lower-energy acoustic phonons. After several steps of this decay, the phonon wave number will be $< 2k_F$, but as they decay, the phonon distribution is expanding spatially. It is not clear whether phonons with $q < 2k_F$ will be produced rapidly enough to enhance the phonon wind. Experiments[15,7] have shown that this is not likely to be a significant source; the number of optical phonons produced per photon was varied by a factor of 4, by varying the photon frequency, without affecting the size of the EHD cloud. An estimate of the magnitude of the phonon wind due to this source (Appendix C) cannot rule it out all together. However, since ΔE_0 is an adjustable parameter, these phonons can be included with the T phonons (for distinction they are called T_{II} as opposed to the primary, or T_I phonons).

D. Magnitude of the wind

To understand how fast the carrier thermalization occurs, a simplified model is presented in Sec. IV A; the e-h system is assumed to be spatially uniform inside a volume which expands diffusively in time. The optical-phonon cascade is assumed to be so fast that new pairs have an initial energy ΔE_0; furthermore, carrier-carrier collisions, while slow compared to optical-phonon emission, are sufficiently rapid to give the carriers a common temperature, and a Boltzmann distribution in energy (or a Fermi-Dirac distribution in the condensed phase). Given this model, the temporal evolution is solved numerically, using exact expressions for the acoustical-phonon emission rates. It is found that the phonon wind reaches an almost steady-state value even before the e-h gas has cooled to its liquid condensation temperature (~10 nsec after the laser beam initially strikes the surface); after condensation the wind rapidly attains a somewhat higher value, due to the binding energy of the liquid. Furthermore, the final equilibrium carrier temperature is quite close to the lattice temperature, as observed experimentally.

In Sec. IV B a similar calculation is made to estimate the temperature distribution of carriers near the crystal surface (assuming the e-h pair density is uniform). It is found that, at the higher power levels used experimentally, the gas temperature may exceed 10 K very near the surface, but cools rapidly to the lattice temperature in a distance smaller than the laser spot radius (assumed to be $r_l \sim 100$ μm). A by-product of this calculation is the *exact emission spectrum* of T phonons. This spectrum can be used in conjunction with the results of an earlier study[10] to generate both the *magnitude* and the *anisotropy* of the phonon wind, both in good agreement with experiment.

Finally, some related topics are discussed in Sec. V. The difficult problem of the droplet velocities measured by Doehler *et al.*[16] is discussed in Sec. V A. Their measurements showed no evidence of T phonons. However, to analyze the velocity data close to the crystal surface, it is necessary to know what happends to phonons which strike that surface. Because a fraction of them are absorbed or diffusely scattered, the R phonons will produce a net flux *into* the surface which could mask the smaller T-phonon flux.

Keldysh[1] showed that the R phonons would also produce a repulsive interaction between droplets which would limit the maximum possible drop size (in unstressed Ge). In Sec. V B it is shown that this estimate of the R-phonon wind is in agreement with other values. Taking all the data

together, it appears that there may be five times as many R as T phonons.

II. KINETIC EQUATIONS

Keldysh[1] showed that the long-wavelength phonons produce a repulsive force $\vec{f}$ between the phonon source and an e-h pair in a drop, of the form $\vec{f} = +A\vec{r}/r^3$, where r is the distance from the source to the drop—the $1/r^2$ falloff is geometrical, due to the spreading out of the phonons. Since droplet motion is damped by electron-phonon collisions in a time $\tau_{ep} \sim 10^{-9}$ sec $\ll \tau_0 \sim 40$ μsec, the velocity of a drop will be

$$\vec{v} = \frac{\tau_{ep}}{m} \sum_{\text{sources}} \vec{f}, \tag{1}$$

where the sum is taken over all sources of phonons. The cloud kinetic equations are then completed with the continuity equation

$$\frac{\partial n}{\partial t} + \vec{\nabla} \cdot (n\vec{v}) = -n/\tau_0, \tag{2}$$

with n the average e-h pair velocity in the cloud (in general $n \ll n_0$).

In a typical experiment, the laser is focused to a small disk ($r_l \sim 100$ μm) on the crystal surface and an approximately hemispherical cloud of EHD's grows from this region. (Actually, the cloud has rather complicated fine structure associated with crystal symmetry directions, due mainly to anisotropy in the electron-phonon scattering rate and to phonon-focusing effects,[7,10] but these effects will be ignored in the present calculation.) This geometry is here simplified by assuming spherical symmetry. The T phonons are assumed to be produced uniformly inside a sphere of radius r_l; the density n is assumed to be a constant n_l inside this sphere, and determined by Eqs. (1) and (2) outside of it.

The above assumption greatly simplifies the description of the R phonons. (As discussed in Sec. V A, it corresponds to specular reflection of phonons at the crystal surface and hence *overestimates* the effectiveness of R phonons in producing the EHD cloud.) Using Gauss's theorem, the velocity v may be rewritten

$$v = \frac{1}{\tau_0 r^2}[\gamma_T N_\infty + \gamma_R N(r)]. \tag{3}$$

Here

$$N(r) = 4\pi \int_0^r n(r') r'^2 \, dr' \equiv \frac{4\pi}{3} r_l^3 \hat{n}$$

is the total number of e-h pairs localized within the distance r of the origin, and

$$N_\infty = \lim_{r \to \infty} N(r) \equiv \frac{4\pi}{3} r_l^3 \bar{n}$$

is the total number of pairs produced. The strength of the phonon wind is measured by the constants γ_T (the T-phonon contribution) and γ_R (from R phonons). These constants represent the contribution to the phonon wind due to the thermalization (or Auger recombination) of a single electron-hole pair. They are approximately proportional to the total energy per pair emitted as long-wavelength acoustic phonons (see Appendix A). The magnitude of γ_T is estimated theoretically in Sec. IV.

In steady state, Eqs. (2) and (3) can be solved exactly:

$$2\gamma_R n_l = \left[\left(\gamma_T \bar{n} + \frac{1}{4\pi}\right)^2 + \frac{\gamma_R \bar{n}}{\pi}\right]^{1/2} - \left(\gamma_T \bar{n} + \frac{1}{4\pi}\right), \tag{4}$$

$$\frac{1}{4\pi}\left[\left(\frac{r}{r_l}\right)^3 - 1\right] = -(\gamma_T + \gamma_R)\bar{n} \ln\left(\frac{\bar{n} - \hat{n}}{\bar{n} - n_l}\right) + \gamma_R(n_l - \hat{n}), \tag{5}$$

$$4\pi n = \frac{\bar{n} - \hat{n}}{\gamma_T \bar{n} + \gamma_R \hat{n}}. \tag{6}$$

For $\gamma_R \to 0$, this solution reduces to that of Keldysh[1]: $n = n_l \exp[-(r^3 - r_l^3)/\lambda^3]$, $\lambda^3 = 3\gamma_T N_\infty$. As long as $\gamma_T \neq 0$, n_l saturates: $n_l \xrightarrow{\bar{n} \to \infty} n_{l0} \equiv (4\pi\gamma_T)^{-1}$, and the volume of the cloud increases linearly with pumping intensity $\propto N_\infty$. This behavior is observed experimentally,[3] with $n_{l0} \simeq 10^{15}$ cm^{-3}. In contrast, if $\gamma_T = 0$, n_l does not saturate, but increases in proportion to $\sqrt{N_\infty}$. Correspondingly, the size of the cloud does not grow with N_∞; for large values of N_∞, $n = n_l/2$ at $r^3 = 2.5 r_l^3$. The parameter λ is a convenient measure of the pumping intensity; the total number of carriers produced, N_∞, will exactly fill a spherical cloud of radius λ and volume n_{l0}. Figure 1 shows a variety of density profiles for different choices of γ_T, γ_R, while Fig. 2 shows the laser power dependence of the cloud radius (taken as that value of r for which $n = n_l/2$). The R phonons act to broaden out the cloud, produce a tail in the distribution at larger r, and hence reduce the radius at which $n = n_l/2$. However, except near $r \simeq r_l$, they have little effect on the shape of the r vs power curves.

In most experimental observations of the cloud, the data presented (whether luminescence intensity[17] or absorption of a far-ir probe[3]) are actually characteristic of a cross-sectional profile of density across the entire cloud. Hence in general, the theoretical curves $n(r)$ must be numerically integrated to give curves of intensity versus position before comparing them with experiment (see Sec. III A). However, Mattos *et al.*[3] used an Abel-transform technique to generate experimental $n(r)$ curves. These data are compared to

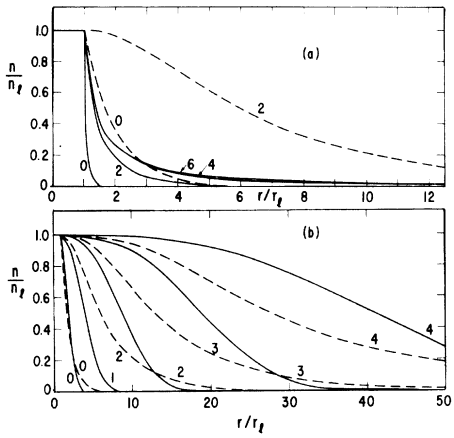

FIG. 1. Spatial profiles of clouds, for several values of γ_R/γ_T: $\gamma_T=0$ [solid lines in Fig. 1(a)], $\gamma_R/\gamma_T=0.05$ [solid lines in Fig. 1(b)], and $\gamma_R/\gamma_T=5$ (dashed lines in both figures). The numbers on the figure give the logarithm of the laser absorption intensity, in relative units.

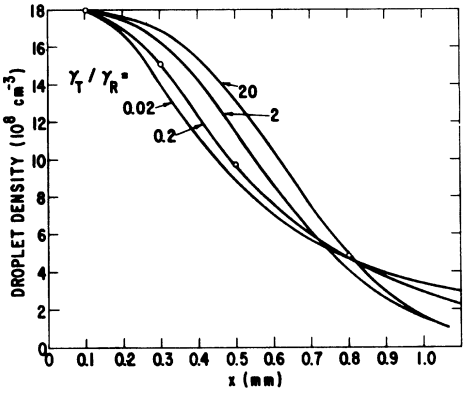

FIG. 3. Spatial profile of clouds. Dots are data of Mattos *et al.* (Ref. 3) for droplet density as a function of depth into the crystal. Solid lines are theoretical predictions for four values of γ_T/γ_R, adjusted in peak height to agree at $x=100$ μm. Power levels: $\lambda^3=400$ ($\gamma_T/\gamma_R=20$), 350(2), 700(0.2), 4000(0.02).

theory in Fig. 3, and suggest a value $\gamma_T/\gamma_R \simeq 0.2$. Other estimates of γ_R are given in Sec. V B.

III. TIME-DEPENDENT SOLUTIONS

A. Cloud buildup after step excitation

Much more information can be found from a study of the time dependence of the EHD cloud buildup. Since the R phonons are produced directly from the EHD's, they will come to equilibrium with the time constant of the EHD, τ_0. However, the T phonons reach steady state with a time constant which is approximately the carrier thermalization time, much less than 1 μsec. In studying the EHD cloud buildup, then, it is a reasonable approximation to assume that the T phonons appear instantaneously, and that the number of R phonons grows with n.

The growth of the cloud may be found by directly solving the flow equations (2) and (3). However, it can be found more elegantly by the following method. First, assume that R phonons can be neglected. Then, if an e-h pair is formed at time t, at $r_1 \leq r_l$, its position as a function of time is specified by

$$\int_{r_1}^{r} dr'/v = t - t_1 . \tag{7a}$$

In the present case, if $r_1 = r_l$,

$$r^3 - r_l^3 = \lambda^3 (t - t_1)/\tau_0 . \tag{7b}$$

If, for $t>0$, drops are produced uniformly in the region $r<r_l$ at a rate G per unit volume, then the number of drops which flow into the region between r and $r+\Delta r$ at the time t is

$$4\pi r^2 n(r,t)\Delta r = \frac{G}{v}\Delta r \int_{r_{\min}}^{r_l} 4\pi r'^2\, dr' \exp[-(t-t_1)/\tau_0] . \tag{7c}$$

This is a sum over drops produced at r' at the time $t_1(r')$; $r_{\min}$ is defined by $t_1(r_{\min})=0$. If $r_{\min}(r) \geq r_l$, e-h pairs have not yet reached r, and $n=0$; once $r_{\min}(r)=0$, $n(r)$ no longer changes with time. (Technically, since G is assumed uniform over $r \leq r_l$, there is no net force on particles at $r=0$, so $v_{\min}$ never equals 0. However, this is not a problem in practice; only about 10% of the pairs form in the region $r<r_l/2$.)

Hence, at any time t, the cloud can be divided into three regions: (a) one in which EHD's have not yet penetrated ($n=0$), (b) a transitional region ($r_l > r_{\min} \geq r_l/3$), where the density n is rapidly changing, and (c) an equilibrium region ($r_{\min} \leq r_l/3$), where the density has essentially attained its

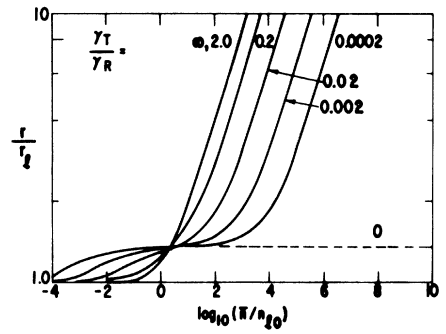

FIG. 2. Power dependence of cloud radius, assuming different values of γ_T/γ_R. (Dashed line $\gamma_T \to 0$ limit.)

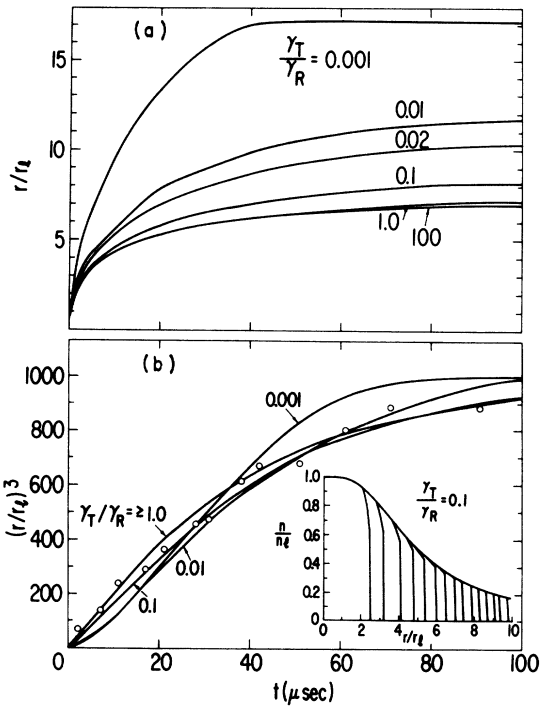

FIG. 4. (a) Growth of cloud after step excitation at $t=0$. All spectra chosen to have $\lambda=1$ mm and $4\pi n_{l0}\gamma_T=1$. (b) Comparison of theoretical buildup to data of Greenstein and Wolfe (Ref. 7) (●). The data are plotted as r^3 vs t to show linear region for small t. In all cases λ was adjusted to give the same final cloud radius. Insert: profiles of $n(r)$ at several times t after the laser is turned on ($\gamma_R=10\gamma_T$). Narrowest profile corresponds to $t=0.5$ μsec; for subsequent profiles t varies from 1 – 14 μsec in 1 μsec intervals.

steady-state value. [Letting $r_{\min}=0$, $t_1=t(r_l)$ in Eq. (7) yields the previous solution, Eqs. (4)–(6) with $\gamma_R=0$.] The above argument is valid only for $\gamma_R=0$, but a direct numerical integration of Eq. (2) shows that a similar sharp front is also present when $\gamma_R\neq 0$ [see insert in Fig. 4(b)].

If the equilibrium cloud radius is much greater than r_l, the transition region can be quite abrupt. If its width can be ignored, then it is quite straightforward to calculate the time evolution of the cloud. First, the leading edge of the cloud can be calculated from Eqs. (3) and (7a) letting $t_1=0$, and $N_\infty(t)=N_\infty[1-\exp(-t/\tau_0)]$:

$$r_{\text{edge}}^3=r_l^3+(3N_\infty/\tau_0)\times\{(\gamma_T+\gamma_R)t-\gamma_R\tau_0[1-\exp(-t/\tau_0)]\}\ . \quad (8)$$

Then, if the transition region is taken to be perfectly sharp, the cloud density will have its equilibrium value [Eqs. (4)–(6)] for $r\leq r_{\text{edge}}$, but $n(r)=0$ for $r>r_{\text{edge}}$. In order to compare this with experiment, the resulting $n(r)$ must be integrated over an appropriate cross section. For instance, Greenstein and Wolfe[7] formed an image of the cloud luminescence on the entry slit of their monochromator. By translating the image across the slit, they produce a one-dimensional intensity profile of the cloud, or a "slit scan."[17] Figure 4(a) shows the time development of the theoretical full width at half maximum (FWHM) of such slit-scan profiles, for fixed values of pumping level and γ_T, but for a variety of ratios γ_T/γ_R. Two points should be particularly noted: (1) r_{edge}, and consequently the FWHM, is proportional to $t^{1/3}$ at short times [Eq. (8a)], (2) the final FWHM depends only weakly on γ_R being only doubled as γ_R varies from 0 to $100\gamma_T$. Figure 4(b) compares the theoretical formula to the data of Greenstein and Wolfe.[7] The pumping intensities have been adjusted so that all profiles have the same equilibrium FWHM and the data are plotted as r^3 vs t, as suggested by Eq. (8). The experimental curve has not been corrected for slit broadening or time-resolution (~5 μsec) broadening, so that an unambiguous choice of γ_R/γ_T cannot be made. However, it appears that the correct value is in the range $\gamma_R\leq 10\gamma_T$, while $\gamma_R\geq 100\gamma_T$ can be ruled out.

The data in Refs. 3, 7, and 17 are all consistent with an average pair density in the cloud $n\simeq 10^{15}$ cm^{-3}. Taking this as equal to n_{l0} gives a value $\gamma_T=8\times10^{-17}$ cm^3. The cloud buildup data of Ref. 7 give an independent measure $\gamma_T\sim 4$–8×10^{-17} cm^3. These experiments are generally performed at fairly low power levels, the absorbed power ≤100 mW. (From Sec. IV, the carrier density at condensation—$t\simeq 20$ nsec—is $\leq 5\times10^{15}$ cm^{-3}.)

It should be noted that the value $n=10^{15}$ cm^{-3} is somewhat of an idealization: by comparing Figs. 23 and 28 of Ref. 17, it can be seen that the cloud *volume* grows linearly with absorbed laser power, while the integrated luminescence intensity (total *number* of e-h pairs) increases *superlinearly*. This is readily understood; at lower power levels, surface trapping reduces the number of pairs, and yet the trapped carriers produce a number of T phonons comparable to the number produced by free carriers. At fairly high power levels, the traps are saturated and the intensity increases linearly with power. It is in this regime that the density $n=10^{15}$ cm^{-3} is measured.

B. Pulsed excitation

The present theory may also be used to describe the kinetics of the cloud after a pulsed laser excitation.[8,9] However, it should be anticipated that the physical processes underlying this effect may differ from those of the earlier experiments, due to the much greater intensity of excitation invol-

ved. At the power levels P of Ref. 8 (assuming 30% of P is absorbed by the crystal), the average density at the time of condensation ($t \simeq 10$ nsec) varies from 3×10^{16}–3×10^{17} cm^{-3}. This is between 10 and 100 times the highest levels used in the investigation of part A, and at the highest power exceeds n_0, the pair density inside an EHD. The number of T phonons produced could be greatly enhanced at these densities, due to direct carrier-carrier deexcitation of hot carriers.[12] (A similar effect, enhancing the number of R phonons, was discussed in Sec. I C.)

Since in these experiments[8,9] a cylindrical region of the sample was optically excited, the EHD and T phonons are assumed to be produced instantaneously ($t_{\text{pulse}} \simeq 0.3$ μsec) over a uniform cylinder $\rho \leq \rho_l$. Each then decays with a characteristic time: τ_0 for EHD, τ_{ph} for the phonons. Equation (7) is now more complicated, since $v = v_0 \exp(-t/\tau_{\text{ph}})$, $v_0 = \gamma_T N_\infty/\rho\tau_0$ for $\rho > \rho_l$; $= v_0(\rho_l)\rho/\rho_l$ for $\rho < \rho_l$, and N_∞ is now the number of pairs produced per unit length. Letting $x = \rho/\rho_l$, $x_1 = \rho_1/\rho_l$,

$$\Lambda^2 = 2\gamma_T N_\infty(\tau_{\text{ph}}/\tau_0)[1 - \exp(-t/\tau_{\text{ph}})]/\rho_l^2,$$

then at any time $t > 0$,

$$n(\rho, t) = \begin{cases} n_l \dfrac{x_1}{x} \exp(-t/\tau_0), & x_1 < 1 \\ 0, & x_1 > 1 \end{cases} \tag{9}$$

$$x_1 = \begin{cases} x \exp(-\Lambda^2), & x < 1 \\ \exp[\tfrac{1}{2}(x^2 - 1) - \Lambda^2], & x > 1. \end{cases} \tag{10}$$

Just as observed experimentally, the "cloud" forms as an *expanding cylindrical shell*. The density distribution at several different time delays is plotted in Fig. 5(a). The characteristic shape, with a sharp leading edge, is quite similar to the data of Ref. 8, Fig. 5(b). (The data are time-resolution broadened, especially at short delay times. In the theoretical curve, a similar broadening was achieved by letting the density be constant at the end of the pulse over a cylinder of thickness $\rho_l = 0.65$ mm.) The position of the leading edge is given by $x_1 = 1$ or

$$x^2 = 1 + 2\Lambda^2. \tag{11}$$

This equation was originally derived by Keldysh,[1] who assumed $\tau_{\text{ph}} = \tau_0$, and was used by Durandin *et al.*[9] to measure the R-phonon contribution of the phonon wind, by analyzing the growth of the cylindrical shell at long time delays ($t \geq 12$ μsec) after the laser pulse. In the present notation, they found $\gamma_R = 5\times10^{-16}$ cm^3. Equation (11) is plotted in Fig. 6 along with data from Ref. 8. (The experimental points at $P = 20$ W refer to the peak position, while those at higher powers are the

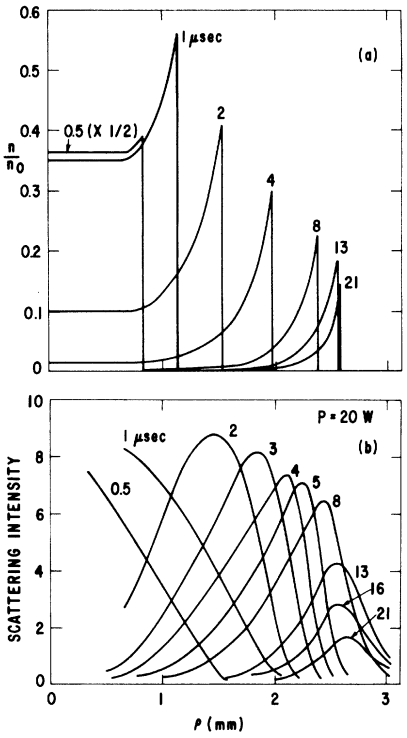

FIG. 5. Temporal evolution of cylindrical shell of EHD formed after pulsed excitation. (a) Theory [Eq. (9)], (b) experiment of Ref. 8.

position of the leading edge.) The theoretical fit for $P = 20$ W assumes $\rho_l \simeq 0$, $\tau_{\text{ph}} = 5$ μsec, $\tau_0 = 40$ μsec, and $\gamma_T N_\infty = 0.15$ cm^2. The theoretical curves for higher powers were found by scaling $N_\infty \propto P$.

Assuming $0.3P$ is absorbed by the crystal, $\gamma_T \simeq 5\times10^{-15}$ cm^3. This number would be smaller if a larger fraction of P were absorbed, and if the R-phonon contribution[9] were factored out. However, it is clear that the value of γ_T needed

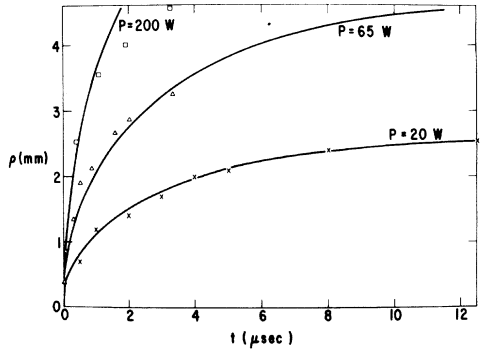

FIG. 6. Growth of EHD shell: peak position versus time. Solid lines represent Eq. (11); data points from Ref. 8.

to describe this data is considerably larger than the value $\gamma_T \simeq 7\times10^{-17}$ cm^3 found from the low-power-absorption regime. Also, the time constant $\tau_{ph}=5$ μsec is much longer than the time required for T phonons to flow ballistically beyond the cloud radius.

There are several mechanisms which may contribute to this enhanced value of γ_T: (1) In the dense plasma, a larger fraction of the thermalization will occur via carrier-carrier collisions, ultimately contributing to the phonon wind. This effect can be even larger than for R phonons, since it is possible for $n>n_0$, and also because the hot carriers cannot escape from the dense plasma as easily as they can from a small EHD. (2) The plasma has a "preferred density" $n_c(T_e)$, corresponding to minimum net pair energy. This is analogous to the average density n_0 inside an EHD; the plasma will tend to expand to maintain $n \lesssim n_c$.[8] This is an expansion mechanism independent of any phonon wind. (3) For cloud radii larger than 1 mm, T_{II} phonons may begin to contribute to the phonon wind (see Table I, below). (4) The relatively slow decay of the T phonon suggests another mechanism. The phonon density may be high enough to bring about a lattice heating[18] or a phonon self-trapping similar to that described by Hensel and Dynes.[5] This could transfer a significant part of the energy emitted as optical phonons into lower-energy phonons capable of interacting with EHD's, and would also cause the phonons to remain localized long after the laser pulse ends.

In conjunction with the above, it should be noted that Manenkov *et al.*[19] directly observed sample heating generated by yttrium aluminum garnet (YAG) laser absorption in Ge (0.1-μsec pulse, $T=1.3$ K). Heat pulses were observed for laser pulse intensities >10 μJ, and decayed relatively slowly (up to 9 μsec at maximum intensity, 100 μJ/pulse). The experiments are not immediately comparable, since in Ref. 19 the sample was heat sunk to a copper plate.

IV. THERMALIZATION PROCESS AND THE MAGNITUDE OF THE PHONON WIND

The above discussion has centered on the kinetic equations (2) and (3), with the properties of the phonons entering only through the parameters γ_T and γ_R. The present section will present a more detailed account of the thermalization process, and in particular, it will be shown that the T-phonon wind is large enough to account for the experimentally observed cloud size. The details of these calculations are presented in Appendices A–D, and are briefly summarized below.

A. Cooling of the electron gas (Appendix A)

The actual coupling of the carriers to both optical and acoustic phonons is known in Ge (see for example Conwell[20]), so the phonon emission spectrum of the electron gas can be calculated as a function of carrier temperature T_e. This allows a calculation of the cooling rate of the gas, as illustrated in Figs. 7 and 8. (A similar calculation for GaAs was given by Ulbrich.[21]) Figure 7 is appropriate to a gas of excitons, while Fig. 8 suggests modifications of the cooling due to condensation. Most of the energy is lost in a rapid emission (~10 psec) of optical phonons, and the curves of Fig. 7 begin at the end of this process—when the energy of a carrier is less than that of a single optical phonon (~38 meV in Ge). To be definite, the parameter ΔE_0, the amount of excess energy the carrier has at the end of the optical-phonon cascade, is assigned a value 7.6 meV (Appendix A) in these calculations.

Figures 7 and 8 also show the rate of emission of energy by acoustic phonons—that is, the T-phonon wind. It can be seen that the wind attains a steady-state value in about an nsec, and

TABLE I. Evolution of T_{II} phonons.

Step	Energy	Lifetime $\bar{\tau}$	Diffusion length L	$\sum\tau$	$(\sum L^2)^{1/2}$
1	$\hbar\omega_{LO}=37.7$ meV	~100 psec	2.8 μm[a]	100 psec	2.8 μm
2	$\hbar\omega_{LA}=18.9$ meV	15 psec	0.1 μm	120 psec	2.8 μm
3	9.1	0.6 nsec	2.5 μm	0.7 nsec	3.7 μm
4	4.4	23 nsec	68 μm	24 nsec	68 μm
5	2.1	0.9 μsec	1.8 mm	0.9 μsec	1.9 mm
6	1.0	36 μsec	51 mm	37 μsec	53 mm

[a] Distance hot carriers travel during phonon cascade, assuming ballistic motion between collisions (and average mass $=m_d=0.22m_0$).

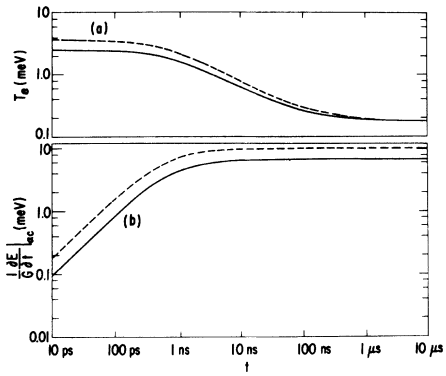

FIG. 7. Thermalization of hot e-h plasma. (a) Electron temperature, T_e vs time. (b) Acoustic phonon emission rate versus time. The solid line represents Ar-ion laser pumping ($\Delta E_0 = 7.6$ meV); the dashed line YAG laser pumping ($\Delta E_0 = 11.3$ meV).

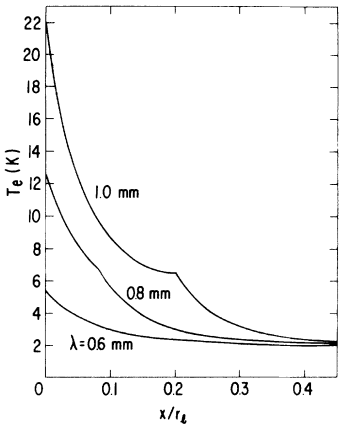

FIG. 9. Steady-state spatial distribution of electron temperature near the laser focus spot. The cloud is assumed to have a constant density ($n = 10^{15}$ cm^{-3}) and the three different power levels are labeled by the radius of the cloud produced.

further, that each e-h pair contributes ~ΔE_0 in energy to the wind.

From Fig. 7, it can be seen that the exciton gas reaches the critical temperature for EHD condensation in a time ~10–100 nsec. This condensation is considered in a simple model in Appendix A; the system, taken to be spatially uniform, is assumed to condense at $T_c = 6.5$ K (in typical cloud experiments the density is well above the threshold value), the system remaining at 6.5 K until all of the gas is condensed (the spike in phonon emission represents the latent heat of condensation), and further cooling takes place at a rate appropriate for a Fermi system. It is not clear whether the enhanced phonon emission will be observable; in reality the system is not spatially uniform (see Fig. 9). Hence condensation will occur first at some distance from the laser spot and gradually at nearer distances, and the enhanced emission will be blurred out. Note that since the EHD's initially condense at a $T_e \gg T$, the average drop radius will initially be larger than its equilibrium value.[22] This effect has been observed experimentally.[23]

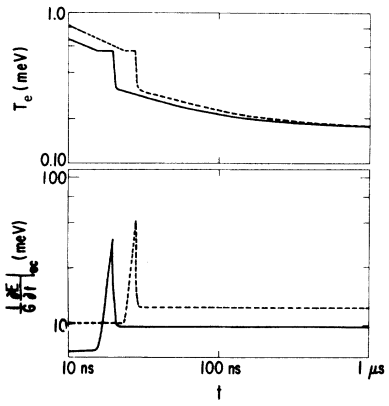

FIG. 8. Condensation of plasma. Similar to Fig. 7, but here gas condenses when $T_e = 6.5$ K. Subsequent cooling is with parameters appropriate to liquid phase.

B. Steady-state temperature distribution (Appendix B)

The temperature distribution of the e-h system is estimated in Appendix B using a simple estimate of thermal diffusivity, and assuming the system has a uniform density. The cooling occurs very near the laser spot, so the system is assumed to be one-dimensional. The results of this calculation are shown in Fig. 9 for a variety of pumping levels. [The pumping level is specified in terms of λ; as defined below Eq. (6), this is the radius of a sphere which would just hold all the carriers if their density were n_{10}.] It can be seen that even for modest pumping levels the gas at the surface can be heated above the critical temperature of EHD's, but that the temperature rapidly drops to the lattice temperature away from the surface.

C. Magnitude of the phonon wind and the anisotropy of the EHD cloud (Appendix B)

In a previous paper[10] on the electron-phonon interaction in EHD's, it was shown how the anisotropic shape of the cloud could be calculated once the distribution in energy of phonons in the phonon wind was known. That paper assumed that the phonons were distributed in a Bose-Einstein distribution at some elevated temperature T_{ph}. While the anisotropy could then be calculated, neither

T_{ph} nor the *magnitude* of the wind were known *a priori*. Both of these can be found using the results of subsection C, and the resulting cloud shape *and size* calculated. The results are shown in Fig. 10 for two different pumping levels, and compared to a calculation assuming $T_{ph}=6$ K. Several features are noteworthy. The anisotropy of the cloud is modified, because of anisotropy in the phonon emission, which, like absorption, is peaked along ⟨111⟩ directions. Hence the broad ⟨111⟩ lobes are enhanced and sharpened, while the ⟨100⟩-directed "flares," caused by phonon-focusing effects,[24] are greatly reduced and smeared out. Also, the radius scales linearly with λ, meaning the cloud volume increases linearly with pumping power, as observed. Finally, the size of the cloud is in good agreement with experiment. Defining an average radius as

$$\bar{r}=\left(\sum_{i=1}^{N} r_i^3/N\right)^{1/3},$$

then $\bar{r}=500$ μm when $\lambda=600$ μm, and $\bar{r}=0.85$ mm when $\lambda=1$ mm. The agreement would be even better if a correction for $\gamma_R \neq 0$ were made—see Fig. 4(a).

The above calculation contains only a single adjustable parameter ΔE_0, and the result can be restated $n_{I0}=(1.3\times10^{16}/\Delta E_0)$ cm^{-3}, where ΔE_0 is in meV. Since the experimental value of n_{I0} is uncertain by about a factor of 2, and the value of γ_R is not well known, this relation cannot yet be used to determine ΔE_0, but a value near 10 meV seems certain—that is approximately the magnitude expected for T_I phonons.

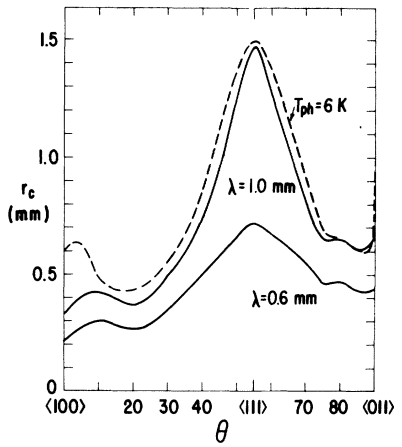

FIG. 10. Anisotropic cloud shape, calculated as in Ref. 10, but using the actual phonon distribution. Dashed line: cloud shape calculated by assuming phonons had a uniform temperature ($T_{ph}=6$ K), as in Ref. 10. Note that the values of λ are input parameters, describing the steady-state number of carriers in the cloud, whereas the distances measured on the abscissa are the outputs of the calculation.

The importance of the linearity found in these calculations ($\gamma_T \propto \Delta E_0$, $\bar{r} \propto \lambda$) should briefly be stressed. At fairly low values of T_e, the acoustic phonons are predominatly created with $q<2k_F$, and the final result, the magnitude of the phonon wind, is insensitive to the detailed form of the phonon distribution. This is fortunate, since a number of steps in the present calculation (thermal conductivity of e-h gas, neglect of T_{II} phonons) could be faulted. If the e–h gas is heated to a sufficiently high temperature, then details of the phonon distribution become important—in particular, a large fraction of the phonons will be produced with $q>2k_F$. The present theory can, in principle, handle this problem since the phonon distribution is calculated explicitly. However, at such high pumping levels many approximations are liable to break down, and the theory must be modified. A rough rule of thumb would be that as long as the cloud volume scales "linearly" with laser power P, the present theory should be applicable. (As mentioned above, surface trapping can result in nonlinear behavior even at small P, but the extension of the theory is trivial.)

D. T_{II} phonons (Appendix C)

The optical phonons generated in the thermalization process decay to form high-energy acoustic phonons, and these in turn generate lower-energy acoustic phonons. In Appendix C an estimate is made of the time it takes these phonons to decay into the wave-number range $\leq 2k_F$. Most of these low-energy phonons will not be produced until the phonons have diffused over too large an area (~2 mm) to effectively interact with the cloud. However, due to the large anisotropy in $2k_F$, strongly interacting phonons with $\vec{q}$ vectors near ⟨111⟩ directions will be produced much sooner. The net energy associated with these phonons is difficult to estimate, but may be comparable to ΔE_0. Since most of them are produced within ~100 μm of the laser spot, they may be treated (in cloud kinetics studies) as T_I phonons, their energy being included in the parameter ΔE_0.

V. ADDITIONAL TOPICS

A. Drop velocities

Figure 4(b) shows very clearly that for $t \leq 40$ μsec, the cloud radius satisfies $r^3 \propto t$. By differentiation, this gives $v \propto 1/r^2$—exactly as ex-

pected for T phonons. This result is in contrast to the results of Doehler *et al.*,[15,16] in which the steady-state droplet velocity was measured directly; their data show a peak in v away from the surface, with smaller values near the surface. The different results found in these two experiments may be due to R phonons; since the R-phonon population grows with a 40-μsec time constant, they would be expected to play little role in the cloud buildup.

If the influence of R phonons is taken into account using the spherically symmetric model of Sec. II, the results of Doehler *et al.* still cannot be understood; for *any* ratio of γ_R to γ_T, the velocity will maximize at the edge of the laser spot.

However, this experiment involves measuring droplet velocities close to the crystal surface, and here the model of Sec. II may break down. The spherical symmetry allowed the use of Gauss's theorem. In particular, in calculating the net force on a particle at distance r from the laser spot, the net effect of all phonons produced at distances greater than r exactly cancels. Near the surface of the crystal this cancellation is possible *only if all phonons which collide with the surface are specularly reflected.* To take an extreme example, if all phonons which collide with the surface are absorbed, then there will be a strong R-phonon wind *into* the surface, which must be balanced by a T-phonon wind. In the case of diffuse reflection the reflected force perpendicular to the surface will be cut in half. In fact, studies of the Kapitza effect suggest that as much as 20% of the longitudinal phonons of energy ~1 meV are directly transmitted into the He bath.[25] Furthermore, Taborek and Goodstein[26] have shown that the elastic anisotropy of Ge leads to significant mode conversion (e.g., longitudinal $\rightarrow$transverse) even among the "elastically" scattered phonons. Since the phonons emitted are predominantly those that are absorbed by droplets (see previous section), any such mode conversion can further weaken the effective specularly reflected wind by a factor ~2.

Such problems of specular reflectivity do not arise for T phonons, which travel ballistically away from the surface.[27] Hence, the effects of nonspecular reflections should have very small effects on the properties of the EHD cloud, except very near the crystal surface, where the T-phonon force is opposed by an R-phonon wind from the bulk of the cloud. In this connection it should be noted that in Ref. 15 it was found that the measured velocity varied by a factor of 2 depending on the location of the laser beam on the crystal surface, while other cloud properties (average size) do not seem to show such sensitivity.

B. Estimates of the magnitude of the R-phonon wind

Whereas the value of γ_T can be determined directly from n_{l0} as $\gamma_T = (4\pi n_{l0})^{-1} \simeq 8 \times 10^{-17}$ cm^3, the value of γ_R cannot be determined directly with any accuracy. In this section a number of estimates are given. While they agree to about a factor of 2, each individual estimate can be faulted and the agreement may be fortuitous. It does seem fairly definite that $\gamma_R \leq 10\gamma_T$, in which case the R phonons can often be neglected in lowest order.

The simplest estimate comes from Fig. 3, in which the density profile suggests $\gamma_R \simeq 5\gamma_T = 3.5 \times 10^{-16}$ cm^{-3}. Alternately, it should be possible to extract an estimate of γ_R from the expansion of the cloud during decay—after the laser has been cut off and the T phonons have spread beyond the edge of the cloud. Such an expansion was observed both for decay from the steady-state cloud[17] and in pulsed experiments,[9] although only the latter case has been analyzed in detail, yielding (in the present notation) $\gamma_R = 5 \times 10^{-16}$ cm^3. It was found, however, in Sec. III B, that the T phonons appear to leak out of the EHD shell much more slowly than estimated from ballistic motion, and this may contaminate the above estimate.

A somewhat larger value, $\gamma_R = 10^{-15}$ cm^3, was found[28] by measuring the EHD velocities in a situation where the motion should be approximately one-dimensional (and hence the T-phonon contribution less significant). Effects of phonon scattering at the sample surface were ignored, however, introducing some uncertainty in the value.

It is possible to obtain an independent experimental estimate of γ_R. Keldysh[1] showed that, due to phonon-wind forces, drops greater than a certain r_c are dynamically unstable. The R-phonon wind will cause different parts of a drop to repel one another, so that for drops larger than some critical size it becomes energetically favorable for a drop to split into two drops. The critical size can be estimated by minimizing the sum of the phonon-wind-induced self-energy and the surface tension. Since the largest EHD's in unstressed Ge are observed to have $r \sim 10$ μm, this gives an upper limit to the R-phonon intensity: $\gamma_R \leq 3 \times 10^{-16}$ cm^3. As shown in Ref. 29 it is possible that the drop radius is limited by a different mechanism, so the R-phonon intensity may be weaker, but not stronger, than the above estimate.

[It should be possible to prove whether or not the drop size is limited by the phonon wind.[30] In a magnetic field, the recombination current produces a net magnetization inside the drop, which favors large drops and should be large enough to overwhelm the phonon-wind repulsion at modest magnetic fields ($\gtrsim$3 kG).]

C. Conclusions

This paper presents a coherent theoretical framework for understanding both the static and dynamic features of the EHD cloud formed in Ge. Evidence has been presented that T phonons are responsible for many of the characteristic features of the cloud (constant average density, fast initial buildup). In this regard, it should be recalled that the structure observed in the cloud shape near ⟨100⟩-crystal axes[7] is extremely sharp—of the order of the laser spot diameter. Such structure would be washed out if only R phonons produced the phonon wind. The magnitude of the T-phonon wind is estimated theoretically, and found to be in good agreement with experiment. A preliminary estimate of the magnitude of the R-phonon wind is also given.

This paper is in many ways preliminary, and much work is still needed for a thorough understanding of the cloud dynamics. In particular, this paper has dealt predominantly with relatively low levels of laser power absorption. At higher levels a number of new phenomena are expected, including self-trapping of T_{II} phonons[5] and high-density plasma effects near the crystal surface (Sec. III B).

APPENDIX A: THERMALIZATION PROCESS

This appendix presents a simplified calculation of the thermal evolution of the EHD system, from the moment ($t=0$) when the laser is turned on until steady state is attained ($t \gtrsim \tau_0 = 40$ μsec). A similar calculation for GaAs was given by Ulbrich.[21]

The carriers are assumed to have a uniform density over a volume which expands diffusively with time. The initial volume is $A\alpha^{-1}$, where $A = \pi r_1^2$ is the laser spot size and α^{-1} is the absorption length—a function of the photon frequency but generally $\lesssim 1$ μm. The diffusion length is $l = (D_0 t)^{1/2}$, with $D_0 \simeq 250$ cm^2/sec (for free excitons at 4.2 K).[2] (Since diffusion in Ge is dominated by carrier-phonon collisions, this diffusion length does not make sense for times less than an electron-phonon scattering time. This error is small on the μsec time scale of interest.) For constant laser pumping and $t \ll \tau_0 = 40$ μsec, the total number of carriers increases linearly with time, $N = Gt$; if $l \ll r_1$, $n = N/Al \propto \sqrt{t}$. Here $G = P_{abs}/h\nu$, where P_{abs} is the power absorbed from the laser and $h\nu$ is the photon energy.

The initial optical-phonon cascade is assumed to be so rapid that the carriers are produced with only the energy ΔE_0 which is left after the cascade. For direct-gap materials ΔE_0 can be estimated[21] by assuming all optical phonons have the same energy $\hbar\omega_{LO}$ (the Γ-point value[31] is 37.74 meV in Ge).

$$\Delta E_0 = h\nu - E_g + E_x - m\hbar\omega_{LO}, \tag{A1}$$

where E_x is the exciton binding energy and m, the number of LO phonons produced, is adjusted so that $0 \leq \Delta E_0 < \hbar\omega_{LO}$. Such an assumption may not work in an indirect-gap material; the electron must emit a high-$\vec{q}$ phonon to jump from the Γ point to the conduction-band minimum at the Λ point. This phonon (most likely LA or LO) will have an energy ~5–10 meV lower than $\hbar\omega_{LO}(\Gamma)$. Equation (A1) may still be used to get a rough estimate of ΔE_0. Using $E_g = 745$ meV, $E_x = 4.2$ meV, yields: for an argon-ion laser, $h\nu = 2.409$ eV, $m = 44$, $\Delta E_0 = 7.6$ meV; for a Nd: YAG laser, $h\nu = 1.167$ eV, $m = 11$, $\Delta E_0 = 11.1$ meV. In comparison, for an Auger electron $\Delta E_0 \simeq E_g - E_B + \frac{3}{5}E_F - m\hbar\omega_{LO}$, where $E_B = 6.2$ meV is the EHD binding energy, $E_F = 6.1$ meV is the (e-h pair) Fermi energy; so $m = 19$, $\Delta E_0 = 25.4$ meV.

Finally, electron-hole collisions are ignored except insofar as they establish a constant e-h temperature $T_e > T$, the lattice temperature. (The carriers are assumed to have a Maxwell-Boltzmann distribution for $T_e > T_c$, the condensation temperature, and a Fermi-Dirac distribution for $T_e < T_c$.) The electron-hole collision rate can be estimated as $\tau_{eh} \sim 75 T_e^2$ psec inside an EHD,[32] and in a low-density plasma should be comparable to the exciton binding time, $\tau_{xB}^{-1} = 0.9 \cdot 10^{-3} n T_e^{-2}$ cm^3/sec (using the experimental value for Si).[33] (Details of the dynamical balance between free carriers and excitons will be neglected; the time τ_{xB} is in general much less than the condensation time.)

Energy is lost from the system via acoustic- and optical-phonon scattering. The loss rates per carrier were given by Conwell[20]:

$$\frac{1}{N}\left\langle\frac{\partial E}{\partial t}\right\rangle_{op} \simeq -A_0 \exp(-\hbar\omega_{LO}/k_B T_e)\left(1+\frac{3}{4}\frac{k_B T_e}{\hbar\omega_{LO}}\right), \tag{A2a}$$

$$\frac{1}{N}\left\langle\frac{\partial E}{\partial t}\right\rangle_{ac} \simeq -A_a T_e^{1/2}(T_e - T). \tag{A2b}$$

Here $A_0 = D^2(\hbar\omega_{LO} m_d^3/2)^{1/2}/(\pi\hbar^2\rho)$, $A_a = 8\Xi_0^2 m_t (2m_d^3 k_B^3/\pi^3)^{1/2}/(\hbar^4\rho)$, where $\rho = 5.32$ gm/cm^3 is the mass density of Ge, m_d(=0.22m_0 for electrons, 0.356m_0 for holes) is the density-of-states carrier mass, m_t(=0.082m_0) is the transverse mass of the electrons (=m_d for holes), and D and Ξ_0 are deformation-potential parameters listed in Table II. Assuming the electrons and holes are in equilibrium, and writing $E = E_e + E_h = 3Nk_B T_e$, and $k_B T_0 = \Delta E_0$, the time development of T_e is given by

TABLE II. Deformation potential parameters.

	Electrons	Holes
Acoustic	Ξ_d = −12.3 eV (unscreened) [a]	= −3.73 eV (unscreened) [b]
	− 7.1 eV (screened) [c]	−9.0 eV (screened) [c]
	Ξ_u = 19.3 eV [a]	= 0
Optical		
	$D = 6\times10^8$ eV cm^{-1} [d]	7.1×10^8 eV cm^{-1} [e]
From Ref. 24	$\Xi_0^2 = \frac{\Xi_d^2}{3}\left[2+\frac{m_l}{m_t}\left(\frac{\Xi_u}{\Xi_d}+1\right)^2\right]$	

[a] K. Murase, K. Enjouji, and E. Otsuka, J. Phys. Soc. Jpn. 29, 1248 (1970).
[b] H. Fujiyasu, K. Murase, and E. Otsuka, J. Phys. Soc. Jpn. 29, 685 (1970); scalar average made according to Ref. e.
[c] R. S. Markiewicz, Phys. Status Solidi B 83, 659 (1977).
[d] S. Zukotynski and W. Howlett, Solid State Electron. 21, 35 (1978).
[e] J. D. Wiley, Solid State Commun. 8, 1865 (1970).

$$3\frac{\partial T_e}{\partial t}=\frac{T_0-3T_e}{t}-A_0'\exp(-T_{LO}/T_e)\times\left(1+\frac{3}{4}\frac{T_e}{T_{LO}}\right)-A_a'\left(\frac{T_e}{T_{LO}}\right)^{3/2}\left(1-\frac{T}{T_e}\right) \quad \text{(A3)}$$

where $k_BT_{LO}=\hbar\omega_{LO}$, $k_BA_0'=A_{0(e)}+A_{0(h)}=59$ meV/psec, and $k_BA_a'/\nu=0.84$ meV/psec is defined similarly. Here ν is a correction factor which accounts for the deviation of the phonon distribution from equipartition at low temperatures, described in Appendix D, and

$$N_{ph}(T)\equiv[\exp(\hbar c_s q/k_BT)-1]^{-1}\to k_BT/\hbar c_s q$$

at high T. Equation (A3) is integrated numerically and the results shown in Fig. 7 for $\Delta E_0=7.6$ and 11.1 meV. The initial conditions are $T=T_0$ at $t=t_1$, the end of the LO-phonon cascade [$t_1\simeq m\tau_{LO}\simeq\sqrt{m}\,\bar\tau_{LO}$, where[20] $\bar\tau_{LO}=\pi\hbar^2\rho(2\hbar\omega_{LO}/m_d^3)^{1/2}/D^2=1.7$ psec (average for electrons and holes)]. The curves do not change significantly if the optical phonon scattering is ignored.

In the above calculations $T_e=6.5$ K $=T_c$, the critical temperature for drop condensation, in a time ~10–30 nsec. Since the EHD cloud experiments are performed well above the condensation threshold (at $T_e=T\simeq2$ K), the carrier gas will rapidly condense. Ignoring supersaturation, the gas begins to condense when $T_e=T_c$. The condensation occurs at such a rate that the latent heat, k_BT_L is just balanced by phonon emission, so that T_e remains at T_c until the condensation is complete. Here k_BT_L is the difference between the gas and liquid energies per pair, $k_BT_L=3k_BT_e-E_L$, with $E_L=-\phi+\frac{1}{2}\sigma(k_BT_e)^2$, $\phi\simeq2.0$ meV, and

$$\sigma=\frac{\pi^2}{2}\left(\frac{1}{E_{F_e}}+\frac{1}{E_{F_h}}\right)=3.39\ \text{meV}^{-1}\ \text{(Ref. 2)}.$$

Letting x be the fraction of carriers condensed, and ignoring optical-phonon emission, the rate of condensation is

$$T_L\frac{\partial x}{\partial t}=A_a'\left(\frac{T_e}{T_{LO}}\right)^{3/2}\left(1-\frac{T}{T_e}\right)[1+(\alpha-1)x]-\frac{T_0-3T_e+T_Lx}{t}. \quad \text{(A4)}$$

In the above equation α accounts for the enhanced phonon emission in the liquid phase,[34] $\alpha=\frac{3}{8}(\pi T_F/T_e)^{1/2}\alpha_0\simeq1.45\alpha_0$ (average of electrons and holes at $T_e=6.5$ K). The factor $\alpha_0=3.31\nu'/\nu$ includes the effect of screening on the deformation potential Ξ_0 (Table I) and the fact that the correction factor ν' has a different value for a degenerate system (Appendix D). After the system is condensed ($x=1$), the cooling continues, now following

$$\sigma k_BT_e\frac{\partial T_e}{\partial t}=\frac{T_0'-\frac{\sigma}{2}k_BT_e^2}{t}-\alpha A_a'\left(\frac{T_e}{T_{LO}}\right)^{3/2}\left(1-\frac{T}{T_e}\right), \quad \text{(A5)}$$

with $k_BT_0'=(\Delta E_0+\phi)$. The modified cooling curve, taking condensation into account, is shown in Fig. 8. In agreement with most experimental findings, the steady-state heating is quite small, $T_e(40\ \mu\text{sec})\simeq T$. The rate at which energy is transferred to the acoustic phonons is just $-\langle\partial E/\partial t\rangle_{ac}$ and this is also plotted in Figs. 7 and 8.

Two approximations in the above treatment should be briefly discussed. First, a 1:1 relation has been assumed between the number of photons absorbed and the number of e-h pairs produced. In practice, the situation is more complicated due to surface trapping.[21] It is generally observed that at low pumping levels the

EHD luminescence intensity increases superlinearly with laser-pump intensity, gradually approaching a linear rate of increase as the surface traps become saturated (see, e.g., Refs. 17 and 35). This situation can readily be modeled via a system of kinetic equations,[21,35] assuming each trapped carrier contributes an energy $\Delta E_0' (\neq \Delta E_0)$ to the phonon wind. However, the thermalization curve will now depend explicitly on the laser intensity (for a Maxwell-Boltzmann carrier distribution, the cooling per carrier depended only on T_e and not on n). The details of the thermalization will be changed, but the times involved should not vary by more than factors of 2.

The second approximation is to assume a uniform temperature distribution throughout the cloud. This assumption is in fact contrary to the idea that the T_1 phonons are localized near the pumped crystal surface. The situation will be described more fully in Appendix B, where a model of the steady-state spatial distribution of T_e will be given. While the distribution of T_e is significant, the main result, that the phonon wind reaches steady state in a time $\ll 1$ μsec, should remain unchanged.

APPENDIX B: STEADY-STATE PHONON DISTRIBUTION

1. Temperature distribution

For a spatially non-uniform carrier distribution, a term $\vec{\nabla} \cdot (D \vec{\nabla} T_e)$ must be added to the left-hand side of Eqs. (A3) and (A5), where D is the carrier-mediated thermal diffusivity, which may be written in a relaxation time approximation as $D = (2\pi^2/9) k_B T \tau_{ep}/m$. Here τ_{ep} is the electron-phonon relaxation time. For nondegenerate electrons $\tau_{ep}^{-1} = \tau_0^{-1} T T_e^{1/2}$, $\tau_0^{-1} = 3.6 \times 10^8$ sec^{-1}.[36] For degenerate carriers, $\tau_{ep}(T, T_e)$ can be found by the methods of Ref. 10, but in view of the simplicity of the model the same value of τ is used throughout. A simplified version of this equation has been solved numerically for the steady-state distribution ($\partial T_e/\partial t = 0$), and the results are shown in Fig. 9.

The simplifications are as follows: (1) the carrier density is assumed to be spatially uniform, (2) the problem is considered to be one-dimensional. Since the carrier temperature reaches the lattice temperature in a distance $x < r_l$ (the radius of the laser spot), these approximations are reasonable.

The boundary conditions describe the heat input. At $x = 0$, the heat is uniformly distributed over a disc of radius r_l. The boundary condition then is $-D \partial T_e/\partial x = G \Delta E_0/k_B \bar{n}$ at $x = 0$ (G is the generation rate per unit area). There is an additional discontinuity at the condensation surface, $\Delta(D \partial T_e/\partial x) = G T_L/\bar{n}$. Finally, in steady state, the value of T_e at $x = 0$ is adjusted so that $\partial T_e/\partial x \to 0$ as $T_e \to T$. Figure 9 shows the resulting spatial distribution of T_e for three laser intensities. It can be seen that at the higher pumping levels there is a region of hot plasma ($T_e > T_c$) near the surface of the crystal. The thermalization takes place in the region $x < r_l$, thus justifying the model of T phonons in Sec. II.

2. Magnitude of the phonon wind

In an earlier paper,[10] the *anisotropy* of the shape of the EHD cloud was estimated, using the anisotropy of the electron-phonon interaction and the phonon-focusing effect.[24] In this calculation, the T phonons were assumed to be describable by a phonon-distribution function which was proportional to an equilibrium distribution function at some elevated temperature T_{ph}. By generalizing the results of Appendix B1, it is possible to actually calculate the phonon-distribution function, and thereby not only calculate the *anisotropy* of the cloud by also its actual *size*.

The rate at which phonons of wave number q and polarization $\alpha (= L \text{ or } T)$ are produced from the electrons in a single valley is[20]

$$\frac{\partial N_{q\alpha}}{\partial t} = A(\bar{N}_{eq\alpha} - N_{q\alpha}) . \tag{B1}$$

Here

$$\bar{N}_{eq\alpha} = [\exp(-\hbar c_\alpha q/k_B T_e) - 1]^{-1}$$

is the equilibrium phonon distribution at temperature T_e, and $A = A_1 \sigma$, with

$$A_1 = \Xi_\alpha^2 \left(\frac{q}{q^*}\right) \frac{(m_d^3 m_0)^{1/2}}{2\pi\hbar^4 \rho c_\alpha} , \tag{B2}$$

$$\Xi_L = \Xi_d + \Xi_u \cos\theta , \tag{B3a}$$

$$\Xi_T = \Xi_u \sin\theta \cos\theta , \tag{B3b}$$

$$\left(\frac{q}{q^*}\right)^2 = \left(\frac{m_0}{m_t}\right)[\sin^2\theta + (m_t/m_l)\cos^2\theta] , \tag{B3c}$$

$$\sigma = \begin{cases} \dfrac{\bar{n}}{4N_c} k_B T_e \exp(-\hbar^2 q^{*2}/8 m_0 k_B T_e)/(1 + \bar{N}_{eq\alpha}) , \\ \qquad \text{for } T_e > T_c \qquad \text{(B4a)} \\ \dfrac{\bar{n}}{n_0}\eta , \quad \text{for } T_e < T_c \qquad \text{(B4b)} \end{cases}$$

$$\eta = \begin{cases} \hbar c_\alpha q , \quad 0 \le \dfrac{\hbar^2 q^{*2}}{8 m_0} \le E_F - \hbar c_\alpha q \\ E_F - \hbar^2 q^{*2}/8 m_0 , \quad E_F - \hbar c_\alpha q < \dfrac{\hbar^2 q^{*2}}{8 m_0} \le E_F \\ 0 , \quad \text{otherwise} \end{cases} \tag{B5}$$

θ is the angle between $\vec{q}$ and the symmetry axis of the electron valley, and $N_c = 2(m_d k_B T_e/2\pi\hbar^2)^{3/2}$.

A similar expression holds for the holes. In Eq. (B1), $N_{q\alpha}$ can be approximately replaced by $\bar{N}_{q\alpha}$, the equilibrium phonon distribution at the lattice temperature T.

Using the results of the preceding section [$T_e(r)$], the *net* phonon production over the volume $r < r_l$ has been calculated. This distribution is not well described by an effective phonon temperature, and shows the anisotropy of the electron-phonon interaction, i.e., strongest along ⟨111⟩ directions. This acts to enhance the anisotropy of the cloud still further over that calculated in Ref. 10. Given the net rate of phonon production inside the laser spot volume, the phonon flux outside the spot is given by the continuity equation, assuming ballistic flow

$$N_{q\alpha} = \frac{4\pi r_l^3}{3r^2 c_\alpha}\left\langle \frac{\partial N_{q\alpha}}{\partial t}\right\rangle , \tag{B6}$$

where the bracket indicates a volume average.

In calculating the force of the phonon wind, N_q is multiplied by a factor q^4 (see Ref. 10) which greatly emphasizes the importance of high-q phonons. Figure 11 shows the product $N_q x^4$ for a variety of directions in the ⟨110⟩ plane at power levels $\lambda = 0.6$ and 1.0 mm. Here $x = q/2k_{F0}$, and $k_{F0} = (3\pi^2 n_0/4)^{1/3}$ is a scalar average Fermi momentum for the electrons. The great anisotropy is apparent. At the lower power level there is a sharp cutoff at $q = 2k_F(\theta)$, whereas at the higher level a sizeable number of phonons with $q > 2k_F(\theta)$ are produced. This is because the e-h gas is heated to ~20 K near the sample surface (Fig. 9). Since the drops away from the surface are essentially at the lattice temperature, these phonons will not be reabsorbed but will escape from the cloud. It has been postulated[37] that these phonons might severely weaken the T-phonon wind, but they are properly accounted for in the present calculation. Only when $T_e \gg 20$ K will this loss mechanism be significant, but by this point several other approximations in the present calculation will have broken down. Once N_q is known, the cloud shape is calculated exactly as in Ref. 10, and the resulting profiles are shown in Fig. 10. Shown also is the result of the calculation of Ref. 10. The enhanced anisotropy found by using the actual phonon distribution is apparent.

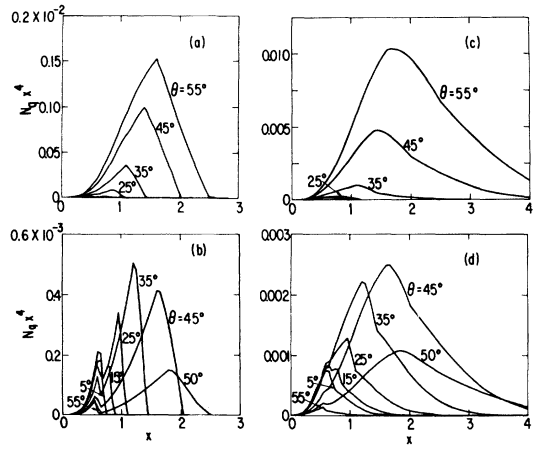

FIG. 11. Anisotropy of T-phonon emission: (a) longitudinal phonons ($\lambda = 0.6$ mm), (b) transverse phonons ($\lambda = 0.6$ mm), (c) longitudinal phonons ($\lambda = 1.0$ mm), (d) transverse phonons ($\lambda = 1.0$ mm). The quantity plotted, as discussed in the text, is $N_q(\Theta)x^4$, where N_q is the (occupation) number of phonons emitted from the thermalizing carriers in the direction Θ, and Θ is defined as in Fig. 10. For $55° < \Theta < 90°$ the curves are approximately the same as those with $\Theta' = 110° - \Theta$.

APPENDIX C: T_{II} phonons

The optical phonons initially emitted by the hot carriers rapidly decay into a pair of LA phonons. These phonons have too high an energy to interact directly with EHD pairs, and must go through several stages of decay to produce effective ($q \leq 2k_F$) T_{II} phonons. To understand the kinetics of T_{II}-phonon production, it is necessary to have a detailed model for the decay of a phonon into two other phonons.

Several calculations[38,39] have related this decay time to the third-order elastic constants of Ge. Since these are known,[40] it should be possible to calculate these rates exactly. The present section will present a highly simplified version of these calculations. The dispersion of the acoustic phonons in Ge will be neglected; the longitudinal (LA) phonons will be characterized by a common velocity $c_L = 5.4 \times 10^5$ cm/sec, the two transverse (TA) phonon branches will be assumed degenerate, with velocity $c_T = 3.25 \times 10^5$ cm/sec. Only normal scattering processes will be considered. All these assumptions are reasonable since the highest allowed q values are only about halfway to the edge of the first Brillouin-zone boundary.

In this case the allowed scattering processes are $L \rightarrow TT$, $L \rightarrow LT$. The elastic constants of Ge will be approximated by those of an elastic continuum, as in Ref. 39. The appropriate coupling constants are given by Eqs. (5b) and (5c) of Ref. 39. When these are averaged over the direction of the initial phonon, the resulting expressions are found to depend slightly on q'/q, the ratio of the wave number of one of the emitted phonons to that of the initial phonon. In the absence of this effect, the most likely decay would be into two phonons of approximately equal energy. The coupling constant may then further be simplified by as-

suming that this holds exactly. This finally gives an average coupling constant independent of energy, which can be written

$$A_{L\to LT}=\left(\frac{10}{3}\right)^{1/2}\frac{2\rho c_L c_T}{\omega_D a}(c_L\gamma_L)\,. \tag{C1}$$

For $A_{L\to TT'}$ the quantity in parentheses is replaced by $c_T\gamma_T$. Here $\rho=5.32$ gm cm^{-3} is the density of Ge, $a=5.66$ Å is the lattice constant, $\hbar\omega_D=32.2$ meV is the lattice Debye energy,[41] and γ is an effective Gruneisen parameter. Using the numerical values of Ref. 40, $\gamma_L=3.84$, $\gamma_T=0.915$. With the above value for A, the decay rate can be written[42]

$$\tau_{L\to LT}^{-1}=\frac{4\gamma_L^2 a\hbar\omega^5}{9\pi M c_L c_T^2\omega_D^2}I_L\,. \tag{C2}$$

Here M is the atomic mass of Ge and

$$I_L/15=\int_a^b y^2(1-y^2)dy\,,$$

with $b=1$, $a=(x-1)/(x+1)$, and $x=c_L/c_T$. Numerically,

$$\tau_{L\to LT}^{-1}=2.75\times10^4(\hbar\omega)^5\ \text{sec}^{-1}\,,$$

with $\hbar\omega$ in meV. Also $\tau_{L\to LT}/\tau_{L\to TT}=(\gamma_T/\gamma_L)^2 2x^2 I_T/I_L=1/5.1$ [I_T differs from I_L in that $b=(x+1)/2x$, $a=(x-1)/2x$]. The results are consistent with the findings of Orbach and Vredevoe,[38] both as to the magnitude of $\tau_{L\to LT}$ and to the fact that $\tau_{L\to LT}<\tau_{L\to TT}$. (In Refs. 42 and 43 a common value of γ was assumed. This would give $\tau_{L\to TT}<\tau_{L\to LT}$.) This distribution of energy of the phonons produced is given by the integrand of I_L, I_T. This is plotted in Fig. 12. Also plotted are the distributions which would be produced using the energy-dependent values for $|A|^2$. Note that not all values of E' are allowed in a decay; the LA phonon can have an energy no lower than $\frac{1}{4}$ that of the initial phonon (the TA phonon may have arbitrarily small energies, but the probability is quite small). On the average, each of the product phonons has half the energy of the initial phonon.

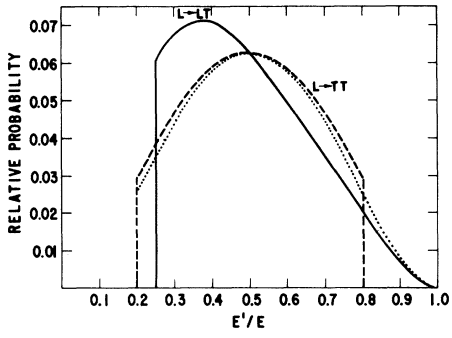

FIG. 12. Distribution in energy E' of phonons produced in a three-phonon decay process as a fraction of the initial energy E. (All curves are normalized to same value at $E'=0.5$ E.) Solid line: energy of L phonon produced in $L\to LT$; dashed line: energy of T phonon produced in $L\to TT$; dotted line: approximation to either of above, using energy-independent matrix element.

Since the TA phonon is on the lowest branch of the dispersion curve, its decay is severely inhibited.[38] In the present calculation, its lifetime will be considered effectively infinite.

The decay sequence of the initial optical phonons can now be estimated. The initial optical phonons decay into two LA phonons, each with half the optical phonon energy, in a time $\tau_0\approx100$–1000 psec.[44] The LA phonons then decay, predominantly to an LA and TA phonon. The spread in energies will be ignored, and each product phonon assumed to have a fixed energy given by the average of the distribution in Fig. 12 ($E'=0.48E$). (Hence each step in the decay sequence has a definite time associated with it.) During its lifetime, each LA phonon (the TA phonons are ignored) diffuses through the Ge, its motion limited by isotope collisions. The mean free path for this collision is strongly energy dependent[45]: $l\simeq100\,\mu$m (3.38 meV/$\hbar\omega$)^4. Table I shows the average progress in each state, with $\bar\tau$ the average decay time and $L=(lc_L\bar\tau)^{1/2}$ the average distance traveled. The $2k_F$ cutoff means that, on the average, phonons will not interact with EHD's unless their energy is ≤0.85 meV [this assumes average values for electrons $k_F=(3\pi^2n/4)^{1/3}=1.2\times10^6$ cm^{-1}, $c_L=5.4\times10^5$ cm/sec; the true value of cutoff energy is anisotropic, having the largest value 2.3 meV along the ⟨111⟩ direction]. Such low-energy phonons will only be produced at the end of step 5, when the T_{II} phonons are spread out over nearly 2 mm. Gauss's theorem may again be applied: the net force on an EHD at a radial distance r is effectively due to only those phonons located at distance $\leq r$. Hence the EHD cloud will only feel the effect of these phonons when it has a radius >1 mm. Thus, while these phonons can enhance the wind on a large cloud they cannot be responsible for producing the cloud in the first place. In the kinetics of the cloud, these phonons will be hard to distinguish from R phonons.

The anisotropy in $2k_F$, however, means that phonons traveling in a ⟨111⟩ direction will contribute to the phonon wind much sooner than the average. Since anisotropy of the phonon decay has been neglected in the above calculations, the effect of these phonons can only be crudely estimated: At the end of step 4, most phonons have an energy ≤2.3 meV (the maximum of $2k_F$), but if they are produced isotropically in a wave vector, only about 10% will be near enough to a ⟨111⟩ direc-

tion. Further, since in each LA → LA + TA process, half the energy is lost to TA phonons, while about one decay in six is into two TA phonons, the net T_{II}-phonon energy, per e-h pair produced is

$$\Delta E_{II} = 0.1 m\hbar\omega_{LO}(0.48)(5.1/6.1)^3$$

$$\simeq 10 \text{ meV} \quad (\text{Ar-ion laser}, \ m = 44),$$

or 2.6 meV (YAG laser, $m = 11$). While this number is very approximate, it is comparable in magnitude to ΔE_0. However, since the phonons are produced in a distance <100 μm from the laser spot, these phonons may simply be lumped in with the T_I phonons, and ΔE_0 treated as an adjustable parameter.

APPENDIX D

The total energy emitted as acoustic phonons can be written as a sum over all phonon modes,[20]

$$\left\langle \frac{\partial E}{\partial t} \right\rangle_{ac} = \sum_{\alpha} \int \frac{dq}{2\pi^2} \hbar c_\alpha q^3 \frac{\partial N_{q\alpha}}{\partial t},$$

where $\partial N_{q\alpha}/\partial t$ is given by Eqs. (B1)–(B5). In the high-temperature limit, the equilibrium phonon distribution can be approximated as $\bar{N}_{q\alpha} = k_B T/\hbar c_\alpha q$, and the results in the text follow, with no correction factor ν. At low temperatures $\bar{N}_{q\alpha}$ deviates from this value, causing the simple expression to overestimate the energy emitted. To estimate a correction factor, the expressions (B1)–(B5) are evaluated numerically for both electrons and holes, and the results added. The computed integrals can to sufficient accuracy be approximated as $T = 2$ K: for a Maxwell-Boltzmann distribution $T_e \geq 6.5$ K

$$\nu = [0.0047 T_e/(1 + 0.0059 T_e)]^{1/4};$$

for a Fermi-Dirac distribution ($T_e \leq 6.5$ K)

$$\nu' = 0.098 T_e(1 - 0.055 T_e) - 0.034.$$

The Fermi-Dirac correction factor interpolates between the high-temperature acoustic-phonon emission rate calculated by Greene,[34] and the low-temperature result of Kogan.[46]

[1] L. V. Keldysh, Pis'ma Zh. Eksp. Teor. Fiz. 23, 100 (1976) [JETP Lett. 23, 86 (1976)].

[2] T. M. Rice, J. C. Hensel, T. G. Phillips, and G. A. Thomas, Solid State Physics (Academic, New York, 1977), Vol. 32.

[3] J. C. V. Mattos, K. L. Shaklee, M. Voos, T. C. Damen, and J. M. Worlock, Phys. Rev. B 13, 5603 (1976), and references cited therein; M. Voos, K. L. Shaklee, and J. M. Worlock, Phys. Rev. Lett. 33, 1161 (1974).

[4] V. S. Bagaev, L. V. Keldysh, N. N. Sibel'din, and V. A. Tsvetkov, Zh. Eksp. Teor. Fiz. 70, 702 (1976) [Sov. Phys.—JETP 43, 362 (1976)].

[5] J. C. Hensel and R. C. Dynes, Phys. Rev. Lett. 39, 969 (1977).

[6] J. Doehler and J. M. Worlock, Phys. Rev. Lett. 41, 980 (1978).

[7] M. Greenstein and J. P. Wolfe, Phys. Rev. Lett. 41, 715 (1978).

[8] T. C. Damen and J. M. Worlock, in *Proceedings of the Third International Conference on Light Scattering in Solids, Campinas, Brazil, 1975* (Flammarion, Paris, 1976), p. 183.

[9] A. D. Durandin, N. N. Sibel'din, V. B. Stopachinskii, and V. A. Tsvetkov, Pis'ma Zh. Eksp. Teor. Fiz. 26, 395 (1977) [JETP Lett. 26, 272 (1977)].

[10] R. S. Markiewicz, Phys. Status Solidi B 90, 585 (1978).

[11] This was originally pointed out by J. P. Wolfe, M. Greenstein, and J. Arzegian, Bull. Am. Phys. Soc. 23, 422 (1978).

[12] Such an effect has been observed in highly photoexcited GaAs: J. Shah, Solid-State Electron. 21, 43 (1978).

[13] Using classical loss formulas [J. D. Jackson, *Classical Electrodynamics* (Wiley, New York, 1962), Ch. 13], it is estimated that for E (carrier) $< 20\hbar_{LO}$, more energy goes into the e-h system than is lost to optical phonons.

[14] The phonons produced in radiative recombination follow a similar decay sequence, but their net contribution to the phonon wind is quite small.

[15] J. M. Worlock, and J. Doehler, Bull. Am. Phys. Soc. 23, 422 (1978); J. Doehler and J. M. Worlock, Solid State Commun. 27, 229 (1978).

[16] J. Doehler, J. C. V. Mattos, and J. M. Worlock, Phys. Rev. Lett. 38, 726 (1977).

[17] J. P. Wolfe, R. S. Markiewicz, S. M. Kelso, J. E. Furneaux, and C. D. Jeffries, Phys. Rev. B 18, 1479 (1978).

[18] M. W. P. Strandberg and L. R. Fox, Phys. Rev. B 17, 3014 (1978).

[19] A. A. Manenkov, G. N. Mikhailova, A. S. Seferov, and V. D. Chernetskii, Fiz. Tverd. Tela (Leningrad) 16, 2719 (1974) [Sov. Phys.—Solid State 16, 1757 (1974)].

[20] E. M. Conwell, Solid State Phys. Suppl. 9 (Academic, New York, 1967).

[21] R. Ulbrich, Phys. Rev. B 8, 5719 (1973), and Solid State Electron. 21, 51 (1978).

[22] V. S. Bagaev, N. V. Zamkovets, L. V. Keldysh, N. N. Sibel'din, and V. A. Tsvetkov, Zh. Eksp. Teor. Fiz. 70, 1501 (1976) [Sov. Phys.–JETP 43, 783 (1976)].

[23] K. L. Shaklee, in *Proceedings of the Third International Conference on Light Scattering in Solids, Campinas, Brazil, 1975* (Flammarion, Paris, 1976), p. 160.

[24] H. J. Maris, J. Acoust. Soc. Am. 50, 812 (1971).

[25] C-J. Guo and H. J. Maris, Phys. Rev. A 10, 960 (1974).

[26]P. Taborek and D. Goodstein, Bull. Am. Phys. Soc. 24, 283 (1979).
[27]Nonspecular reflection can affect only the *magnitude* of γ_T (only by a factor ~ 2), but not the $1/r^2$ form. This is similarly true for γ_R, *outside* the densely populated part of the cloud. However, it is *inside* the cloud that specular reflection (or spherical symmetry) is used to simplify the form of the R-phonon wind (recall the analogy of the gravitational force inside the earth). Therefore, nonspecular reflection will have its strongest effect on the velocities of drops inside the bulk of the cloud.
[28]Ref. 15. In their notation $\gamma_R = \alpha\tau_0/nV$.
[29]R. M. Westervelt, Phys. Status Solidi B 76, 31 (1976).
[30]R. S. Markiewicz, Phys. Rev. B 18, 5573 (1978).
[31]G. Nilsson and G. Nelin, Phys. Rev. B 3, 364 (1971).
[32]A. S. Kaminskii and Ya. E. Pokrovskii, Pis'ma Zh. Eksp. Teor. Fiz. 24, 332 (1976) [JETP Lett. 24, 300 (1978)].
[33]J. Barrau, M. Heckman, and M. Brousseau, J. Phys. Chem. Solids 34, 381 (1973).
[34]R. F. Greene, J. Electron. Control 3, 387 (1957).
[35]J. B. Mock, G. A. Thomas, and M. Combescot, Solid State Commun. 25, 279 (1978).
[36]M. Fukai, H. Kawamura, K. Sekido, and I. Imai, J. Phys. Soc. Jpn. 19, 30 (1964).
[37]J. M. Worlock, J. Doehler, and J. C. V. Mattos, in *Proceedings of the International Conference on Lattice Dynamics, Paris, 1977,* edited by M. Balkanski (Flammarion, Paris, 1978), p. 234.
[38]R. Orbach and L. A. Vredevoe, Physics (N.Y.) 1, 91 (1964).
[39]R. A. H. Hamilton and J. E. Parrott, Phys. Rev. B 178, 1284 (1969).
[40]E.g., H. J. McSkimin and P. Andreatsh, Jr., J. Appl. Phys. 35, 3312 (1965).
[41]C. Kittel, *Introduction to Solid State Physics*, 4th ed. (Wiley, New York, 1971).
[42]Compare M. Roufosse and P. G. Klemens, Phys. Rev. B 7, 5379 (1973).
[43]J. E. Parrott, in *International Conference on Phonon Scattering in Solids, Paris, 1972,* edited by H. J. Albany (CEN, Saclay, 1972), p. 27.
[44]D. K. Ferry, Phys. Rev. B 9, 4277 (1974).
[45]G. A. Slack and C. Glassbrenner, Phys. Rev. 120, 782 (1960).
[46]Sh. M. Kogan, Fiz. Tverd. Tela (Leningrad) 4, 2474 (1962) [Sov. Phys.—Solid State 4, 1813 (1963)].